Three-Dimensional Simulation of Transverse Injection in a Supersonic Flow by the CESE Method

Hao He[1], S.-T. John Yu[2]
Mechanical Engineering Department
Wayne State University
Detroit, MI 48202

ABSTRACT

In this paper, we report numerical simulation of transverse fuel injection in the setting of a scramjet engine. We emphasize on the complex flow structure of the transverse injection into a supersonic cross-flow in the vicinity of the injector. We solve the three-dimensional flow equations by using an extended CESE method. The results shown here are based on a mesh of 5.5 millions cells. The simulations were conducted by using a cost-effective Beowulf cluster. The parallel computing is based on the domain decomposition. The numerical results show complex vortex and shock structure. The results compare favorably with the available experimental data in terms of Mach disk location and penetration depth of the fuel jet.

1. INTRODUCTION

The study of transverse injection into a supersonic stream is important for supersonic combustion ramjet (scramjet) engines. When a gaseous fuel jet is injected into a supersonic crossflow, the fuel acts as an obstruction to the crossflow and produces a strong shock wave. This shock interacts with the boundary layer on the wall to form a complex flow system, in which high and low pressure regions exist in the vicinity of the injector. Figure 1 shows a schematic of the transverse injection, where the jet is sonic and injected perpendicular to the supersonic crossflow. A bow shock occurs due to the disturbance to the incident flow by the transverse injection. The shock strength varies with respect to the distance measured from the injector wall. Away from the wall, the bow shock curves around the injectant plume. Due to the expansion of injected jet and its interaction with the bow shock, complex shock waves are generated in the injectant plume, including a barrel shock and a Mach disk. Due to the blockage to the supersonic cross flow by the fuel injection, a horseshoe vortex tube is formed near the wall. In the injectant plume, a pair of the counter-rotating vortex tubes is also developed.

The trajectory of the fuel jet is of obvious importance in the application of scramjet engines because of the required uniform fuel distribution in the air stream entering the combustor. The jet structure and fuel penetration depend on the jet-to-free stream momentum ratio. Since 1960s, many experiments have been conducted to investigate the effect of the controlling flow parameters to the overall flow field. The free stream Mach number ranged from 1.3 to 4.5 [1-6]. In general, the injection pressure and free stream Mach number are the key factors controlling the overall flow structure. Zukoski et al. [6] and Billig et al. [2] developed equations for calculating the penetration depth and the trajectory, including formulation for predicting the location of the Mach disk, a key feature of the fuel injection. The effect of the static pressure ratio of jet to free stream was formulated based on the concept of an effective backpressure [2-6]. To present the experiments, injectant concentration profiles were presented to describe the trajectory and to verify the theorem [2-6]. Recent works by Gruber et al. [1] also showed the lateral spread of the injectant, which is of great interest to the research on scramjet engines.

[1] Ph.D. Candidate, AIAA Student Member,
Email: haohe@me1.eng.wayne.edu

[2] Associate Professor, AIAA Member,
Email: styu@eng.wayne.edu

Hydrogen and/or heavy hydrocarbons are used as fuels for the scramjet engines. The molecular weights of the fuels employed lead to significant compressible effects in the mixing layer between the injectant stream and the supersonic cross flow. The interactions would directly impact the mixing layer growth rate, flow stability, and turbulent structures and intensity. Therefore, different fuel may affect the potential performance of the scramjets and should be investigated carefully. In previous experiments, injectant includes N_2, He, and Ar. Gruber et al. [1] also used air besides He for the jet in their work. In this work, our simulation follows [1] closely.

The objective of the present paper is to conduct numerical study of the flow field created by sonic transverse injection through a circular nozzle into a supersonic cross flow. The rest of the present paper is organized as follows. In Section 2, we briefly describe basic principle of the CESE method. In section 3, we report the implementation of parallel computing using a Beowulf cluster. Numerical results based on the use of 5.5 millions mesh nodes are shown in Section 4. We then offer concluding remarks and provide cited references.

2. THE CESE METHOD

The space-time CESE Method, originally proposed by Chang [7], is a novel numerical framework for hyperbolic conservation laws. The CESE method is not an incremental improvement of a previously existing CFD method, and it differs substantially from well-established CFD methods. The CESE method has many non-traditional features, including a unified treatment of space and time in calculating flux conservation, the introduction of conservation element (CE) and solution element (SE), a novel shock capturing strategy without using a Riemann solver, and simple treatments for reflective, non-reflective, and no-slip boundary conditions based on a local space-time flux conservation over CEs near the computational boundaries. Details of the CESE method have been extensively illustrated in the cited references [7-10].

To date, numerous highly accurate solutions have been obtained by the CESE method. Based on experience, we found that the CESE method is capable of capturing shocks and acoustic waves simultaneously, where the magnitude of the shock pressure jump could be several orders of that in the acoustic waves. The high-resolution capabilities of the CESE method and the simple boundary condition treatment are critically important to the present calculations.

We note that in the original CESE method, triangular and tetrahedron meshes in spatial domain are used for two- and three-dimensional calculations. Recently, the CESE method has been extended to include quadrilateral and hexahedral meshes in two- and three-dimensional calculations [10]. This extended CESE method is adopted in the present work.

3. PARALLEL COMPUTING

To conduct three-dimensional simulations with millions of mesh grids, we employed parallel computation using a Beowulf computer cluster, which is a PC-based system, interconnected by high-speed networks. The PCs run an open-source UNIX operating system, e.g., Linux in our case. Parallel application programs communicate using industry standard message passing models and libraries, e.g., MPI. By using off-the-shelf PC parts and free software, the parallel computer clusters are fairly affordable.

Effective use of a Beowulf system requires a proper distribution of simulation tasks among the computer nodes. The approach here is to decompose the computational domain into a number of partitions, and to assign each partition to a PC node. The processing nodes execute the same CFD solver but in different sub-domains. They exchange intermediate numerical results at sub-domain boundaries at the end of each iteration time step. Proper domain decomposition would balance the computational workload and memory occupancy of the processing nodes, while minimizing the inter-node communication. In the present work, the computational domain is a simple cube and the domain decomposition could be easily done. For complicate domains, special de-composition tools, such as METIS, could be used.

Different application needs different hardware and different system design. The competition between Intel and AMD bring consumers processors with frequency of up to 3 GHz. However, according to our experience, large memory

bandwidth and fast network are critical to CFD simulations. In two- and three-dimensional calculations, huge amount of double precision data "flow" between computer nodes. Fortunately, recent development of RAMBUS and DDR memory, and Gigabit Ethernet can satisfy our increasing need for fast data transfer.

The Beowulf cluster used in present work consists of eight PC nodes of 2 GHz Pentium 4 CPU, 2 GB PC2100 DDR memory and Gigabit Ethernet controller on each node. The cost of the cluster including the switch is about 20K dollars in the summer of 2002.

4. NUMERICAL RESULTS

The flow conditions are taken from the experimental conditions by Gruber et al. [1]. The free stream is air with pressure P_a = 41.8 kPa, density ρ_a = 0.86 kg/m^3 and Mach number M_a = 1.98. The injectant is also air with pressure P_j = 476 kPa and density ρ_j = 6.64 kg/m^3. The injection Mach number is slightly higher than the sonic condition, M_j = 1.0, to avoid complex boundary condition treatment at the injection port. The diameter of the injector nozzle d = 2 mm. A structured hexahedron mesh of about 5.5 million cells is used in the present calculation. Measurement of length and coordinates are normalized based on the diameter of the injector hole. Numerical solutions of the flow variables were normalized by the free stream values.

Figure 2 shows the two-dimensional pressure contours from the side view. One can clearly observe the bow shock, the barrel shock and the Mach disk. Due to the high-pressure regions in front of the injection hole, the bow shock bends forward in the near-wall region.

Figure 3 shows pressure distribution along the central line of the computational domain on the wall. Note that pressure increases steeply before the injector, and the variation of pressure distribution in front of the injector showed the complex flow structure in the region. In the lee of the injection hole, pressure is lower than the free stream pressure. Further downstream from the injector, pressure recovers to be higher than unity. Although not shown, pressure would asymptotically approach unity in far downstream locations.

Figure 4 shows the vorticity contours on cross sections at various axial locations. The well-known counter-rotating vortex pair is clearly shown. In addition, there are many smaller vortices, and the overall flow pattern is very complex. We remark that the contour plots also show the interactions between the vortex pair and the boundary layer.

Figure 5 shows the two-dimensional vorticity contours at the central plane. Figure 6 shows the top view of the vorticity contours at various heights from the injection plane. From the top view, we can access the lateral spread of the injected jet. The necking of the wake near the wall could be clearly seen. Along the streamwise direction, a lateral contraction of the mixing region occurs, where the mixing layer becomes smaller. These figures show elaborate structure of the flow field.

Figure 7 shows the two-dimensional velocity vectors at the central plane. Similarly to Fig. 2, all salient features of the transverse injection flow field are resolved, including the bow shock, the barrel shock, the Mach disk, and the recirculation regions near the injection hole.

Figure 8 showed the two-dimensional velocity vectors on cross sections at various axial locations. These plots show multiple vortices in the streamwise direction. Moreover, Figure 8 shows a striking three-dimensional shock structure just below the main vortex pair. At x/d = 4, a narrow trapezoidal zone is enclosed by the shock wave. The trapezoidal zone expands in the transverse direction as the fluid flows downstream.

Figures 9-11 show the mass fraction contours of the jet. The main features are very similar to that in the vorticity contours. These plots also clearly show the propagation of the injectant along the boundary layer.

The location of the Mach disk is an important parameter to access the effectiveness of the injection flow field. Using Mach number of the free stream and the pressure ratio as the controlling parameters. Billig et al. developed the following two equations for the Mach disk location [2]:

$$\frac{y_1}{D_j^*} = M_j^{1/4}\left(\frac{p_j^*}{p_{eb}}\right)^{1/2}, \qquad (1)$$

$$\frac{x_1}{y_1} = 1.25\left[1 - \exp\left(-\frac{M_a}{M_j}\right)\right], \qquad (2)$$

where x_1 and y_1 are the coordinates of the Mach disk center. In Eqns. (1-2), M_j and p_j are the Mach number and pressure of the injectant, D_j is the diameter of the hole. The superscript * stands for sonic point condition. M_a is the Mach number of the free stream. p_{eb} = 2/3 p_{ta}' is the effective back pressure, where p_{ta}' is the Pitot pressure behind the shock of the free stream. The Mach disk locations predicted by these two equations are plotted in Figure 12 and Figure 13. The present results, denoted by filled and open rhombuses, compared well with the predictions by Billig's correlations. In the same plots, some of the previous experimental data are also included.

Figure 14 shows the injectant concentration profiles at various streamwise positions. The trajectory is also plotted based on the injectant concentration profiles. Along each injectant concentration profile, the concentration decreases sharply in the region lower than the core of the injected jet.

Lateral spread of the injectant is plotted in Figure 15. We check the maximum width of the concentration contour where the injectant concentration is equal to 10% or 90%, at all streamwise locations. From this figure, we can see that the maximum spread width is reached at the location about 4d from the injection hole. The spread remains about the same with some contraction for locations at $x/d > 4$.

In order to access the numerical accuracy of the present calculation, we conducted another calculation based on the flow conditions reported in [3], i.e., M_a = 2.72, p_j^*/p_{eb} = 2.73, p_{tj}/p_{eb} = 5.18, q_{ji}/q_a = 2.38, where p_{tj} is the total pressure of the injectant, q_{ji} is the initial dynamic pressure of the injectant and q_a is of the free stream. Species concentration profiles at four streamwise positions were investigated, including x/d =2.23, 4.46, 6.70, and 8.92. The concentration profiles and trajectory are shown in Figure 16, where the numerical results are shown in lines and symbols are the experimental data. The comparison between the present CFD results and the experimental data is favorable. In addition, based on the maximum values of the species concentration at each axial location, we also plotted the trajectory of the jet. The trajectory also compared well with the experimental data by Orth et al. [3] and the result predicted by Shetz et al. [5].

5. CONCLUDING REMARKS

In this paper, we reported high-fidelity numerical solutions of the transverse injection into a supersonic cross flow. The calculation was done by using the CESE method, running on a Beowulf cluster. For high resolution, more than 5 millions mesh nodes were used. The numerical results show crisp resolution of complex flow features. In particular, the present results show complex vortex structure in the streamwise direction and a distinct three-dimensional shock structure in the region under the bended jet and the boundary layer. The numerical results compared well with the previous theoretical and experimental data for the Mach disk locations, jet trajectory, and the injectant concentration profiles.

REFERENCES

1. M. R. Gruber, A. S. Nejad, T. H. Chen and J. C. Dutton, "Compressibility effects in supersonic transverse injection flowfields", *Phys. Fluids* 9 (5), pp. 1448, May 1997.
2. F. S. Billig, R. C. Orth, and M. Lasky, "A Unified Analysis of Gaseous Jet Penetration", *AIAA Journal*, Vol. 9, No. 6, pp. 1048, 1971.
3. R. C. Orth and J. A. Funk, "An Experimental and Comparative Study of Jet Penetration in Supersonic Flow", *J. Spacecraft*, Vol. 4, No. 9, pp. 1236, 1967.
4. J. A. Schetz and F. S. Billig, "Penetration of gasesous jets injected into a supersonic stream", *J. Spacecraft Rockets*, 3, pp. 1658, 1966.
5. J. A. Schetz, P. F. Hawkins and H. Lehman, "Structure of Highly Underexpanded Transverse Jets in a Supersonic Stream", *AIAA Journal*, Vol.5, No. 5, pp.882, 1966.
6. E. E. Zukoski and F. W. Spaid, "Secondary Injection of Gases into a Supersonic Flow", *AIAA Journal*, Vol. 2, No. 10, pp. 1689, 1964.
7. S.C. Chang, "The Method of Space-Time Conservation Element and Solution Element –

A New Approach for Solving the Navier Stokes and Euler Equations," *J. Comput. Phys*., 119, pp. 295, 1995.

8. S.C. Chang, X.Y. Wang and C.Y. Chow, "The Space-Time Conservation Element and Solution Element Method: A New High-Resolution and Genuinely Multidimensional Paradigm for Solving Conservation Laws", *J. Comput. Phys.*, 156, pp. 89, 1999
9. S. C. Chang, X. Y. Wang and W. M. To, "Application of the Space-Time Conservation Element and Solution Element Method to One-Dimensional Convection-diffusion Problems," *J. Comput. Phys.*, 165, pp. 189, 2000.
10. Z.-C. Zhang, S. T. John Yu, and Sin-Chung Chang, "A Space-Time Conservation Element and Solution Element Method for Solving the Two- and Three-Dimensional Unsteady Euler Equations Using Quadrilateral and Hexahedral Meshes", *J. Comput. Phys.*, 175, pp. 168, 2002.

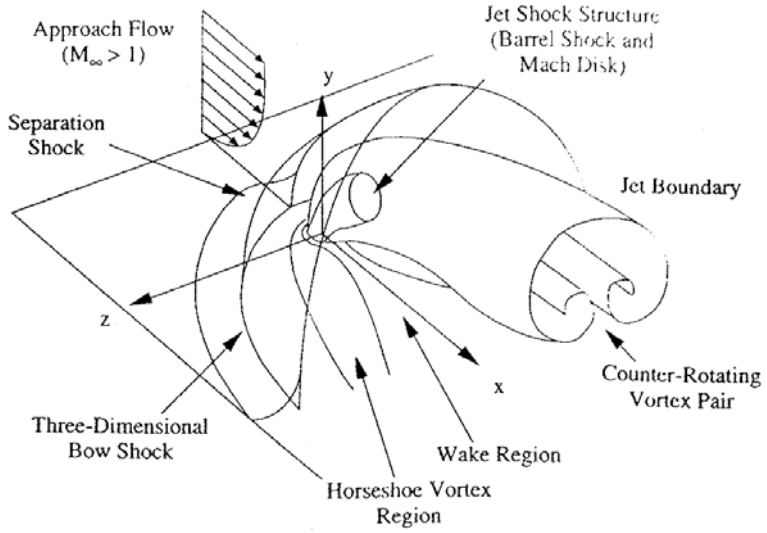

Fig. 1: A schematic of the transverse injection flowfield.

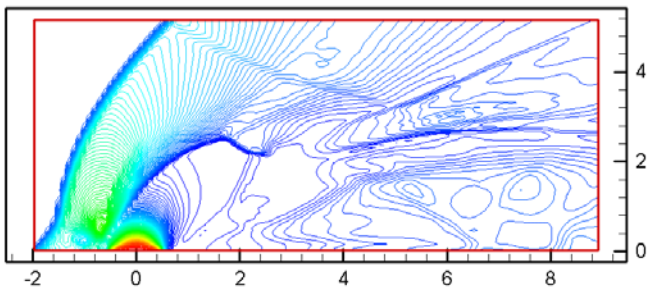

Fig. 2: Pressure contour at the central plane ($y = 0$).

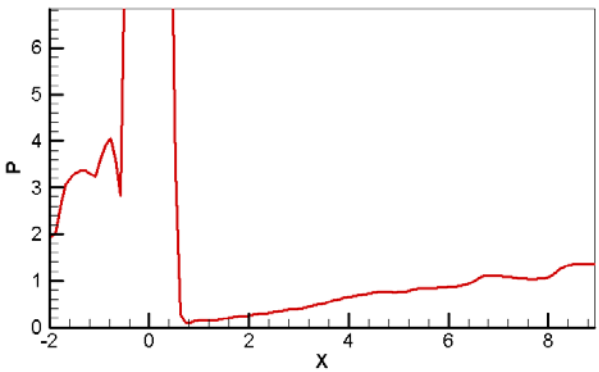

Fig. 3: Pressure distribution at central line along the wall.

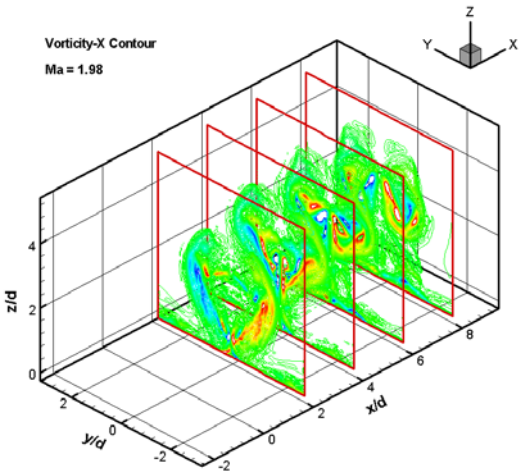

(a)

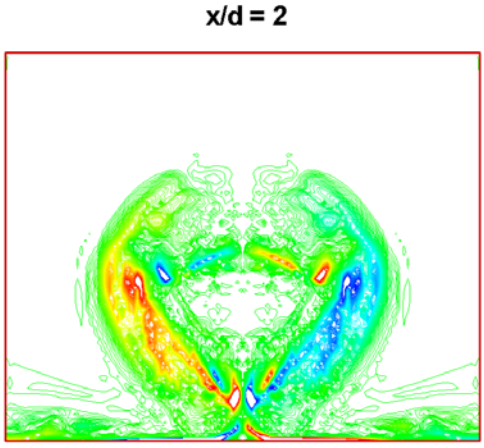

(b)

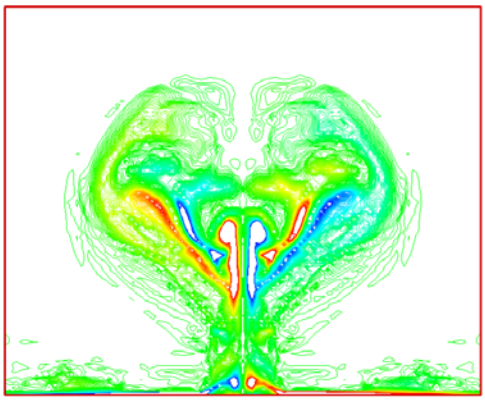

(c)

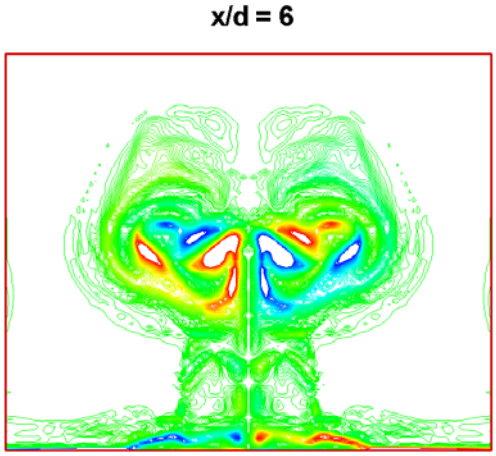

(d)

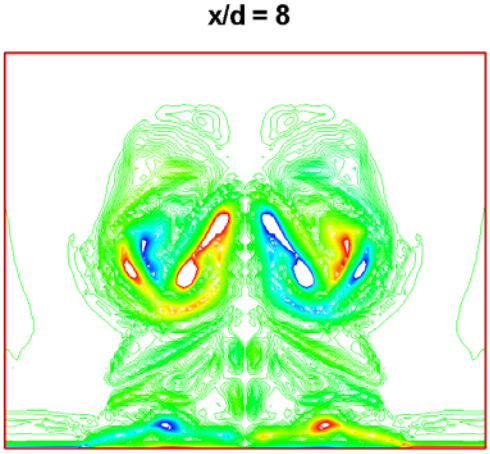

(e)

Fig. 4: Contours of the x-component of the vorticity. (a) The checking plane distribution. (b) $x = 2d$, measured from the center of the injector hole. (c) $x = 4d$. (d) $x = 6d$. (e) $x = 8d$.

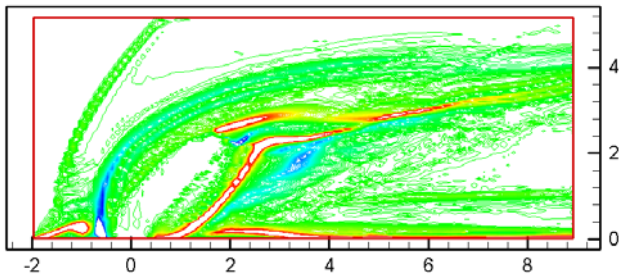

Fig. 5: Contours of the y-component of the vorticity at the central plane ($y = 0$).

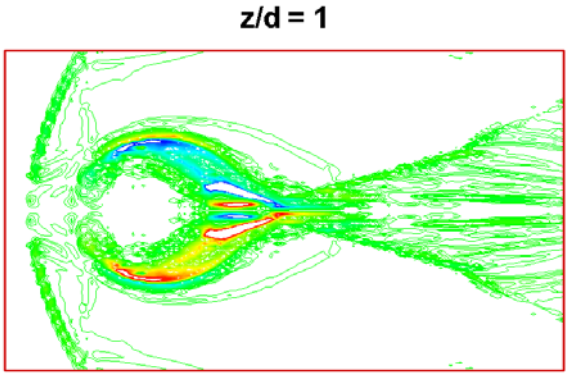

(a)

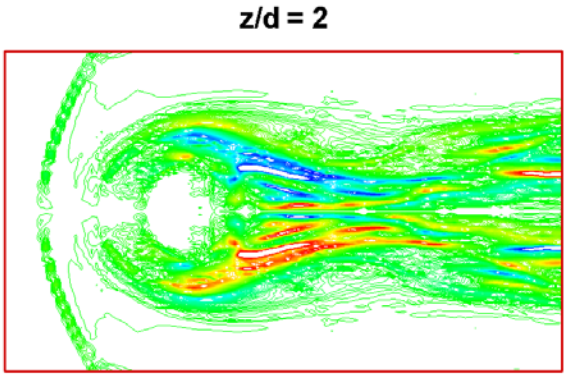

(b)

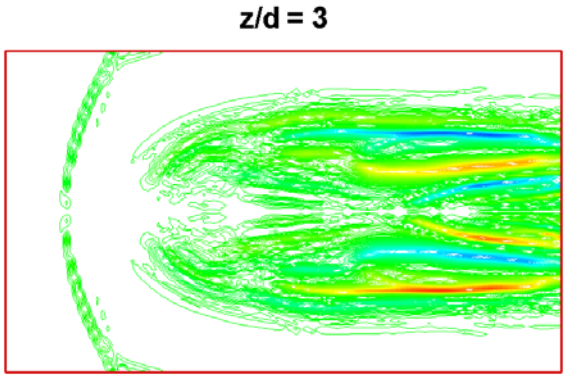

(c)

Fig. 6: Contours of the z-component of the vorticity. (a) $z = d$, above the wall, (b) $z = 2d$, (c) $z = 3d$.

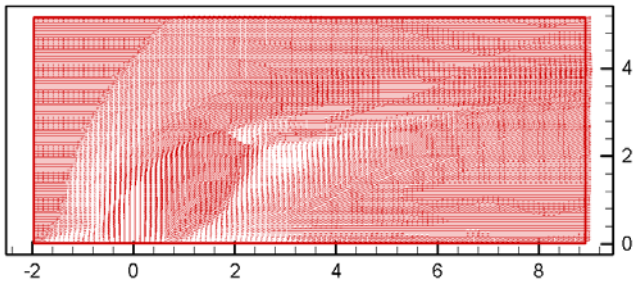

Fig. 7: Velocity vectors at the central plane ($y = 0$).

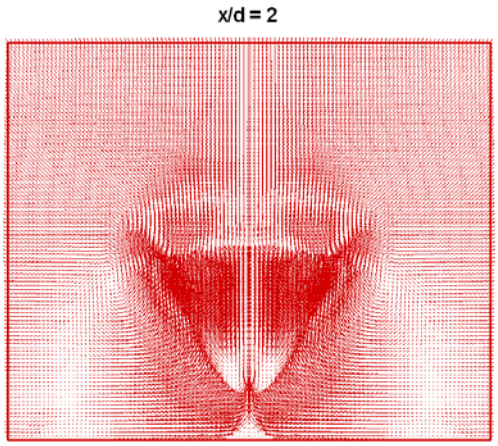

(a)

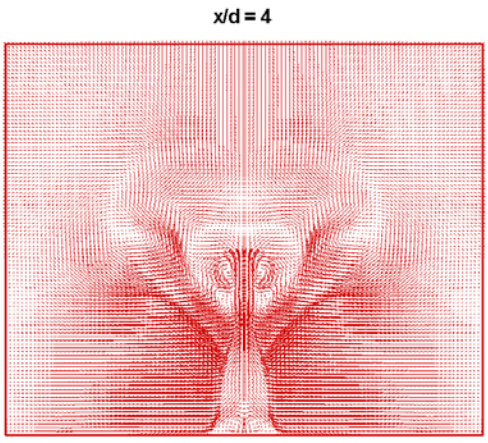

(b)

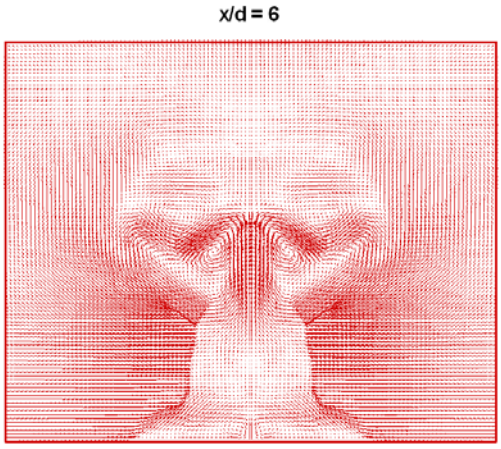

(c)

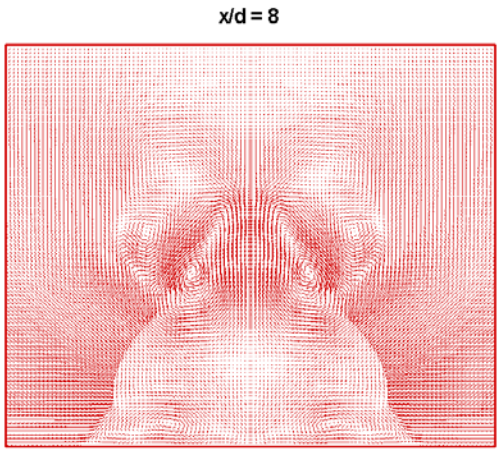

(d)

Fig. 8: Velocity vectors at the cross sections at (a) $x = 2d$ measured from the center of the injector hole, (b) $x = 4d$, (c) $x = 6d$, (d) $x = 8d$.

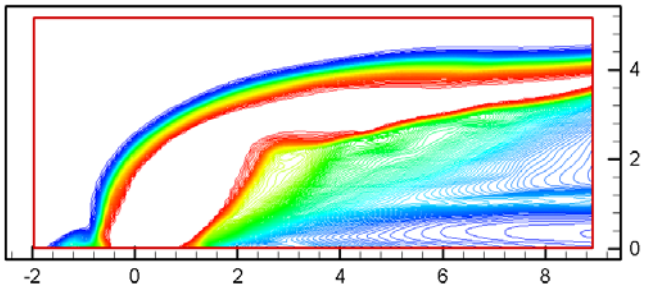

Fig. 9: Injectant concentration contour at the central plane ($y = 0$).

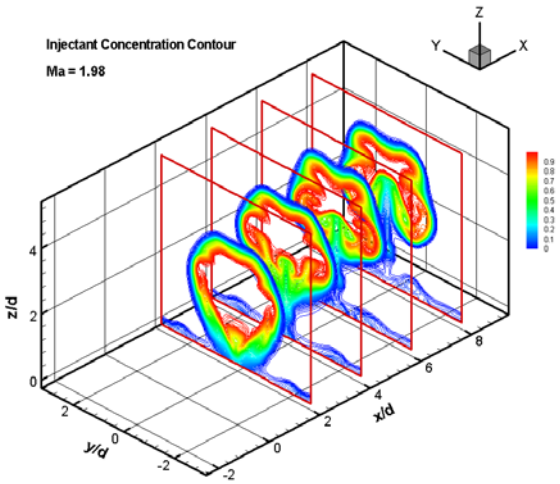

(a)

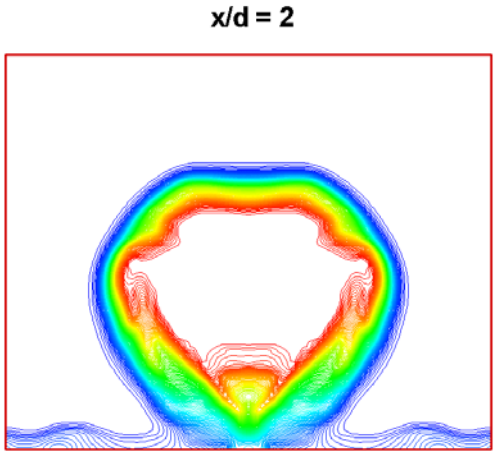

(b)

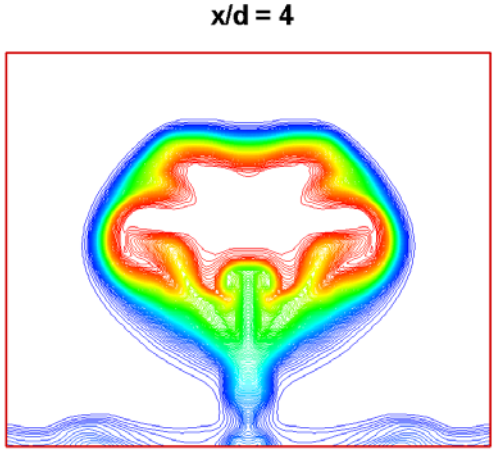

(c)

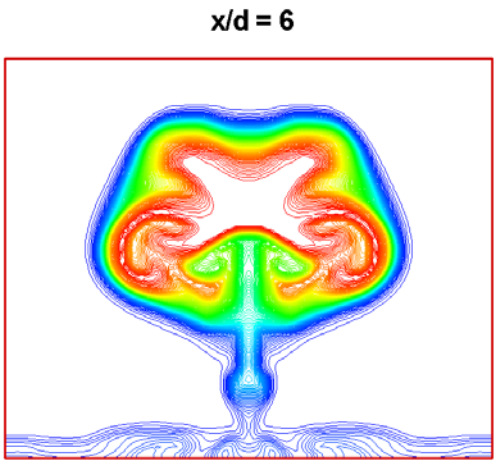

(d)

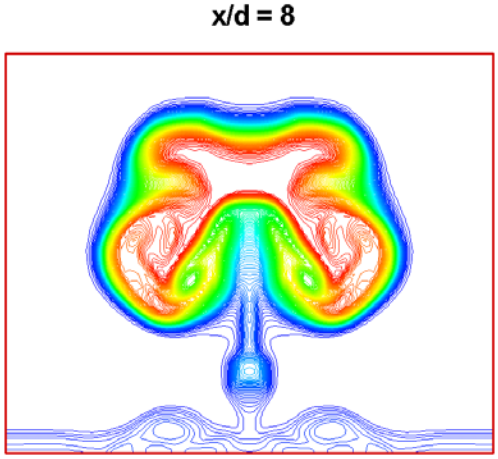

(e)

Fig. 10: Injectant concentration contours on the cross sections in the streamwise direction. (a) The checking plane distribution and the contour legend. (b) $x = 2d$, measured from the center of the injector hole. (c) $x = 4d$. (d) $x = 6d$. (e) $x = 8d$.

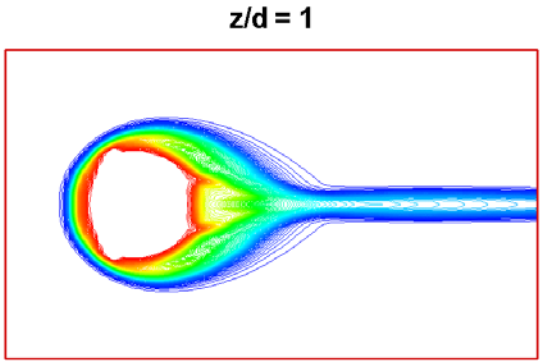

(a)

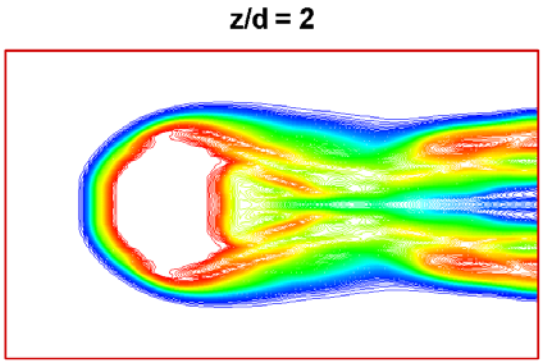

(b)

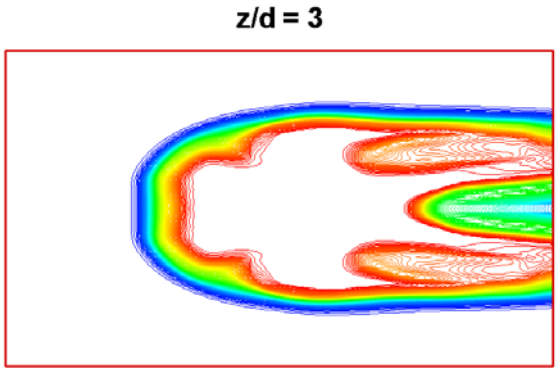

(c)

Fig. 11: Injectant concentration contour at (a) $z = d$ above the wall, (b) $z = 2d$, (c) $z = 3d$.

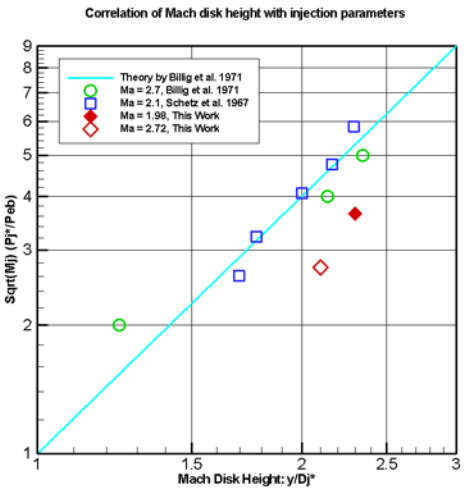

Fig. 12: Mach disk locations as a function of the injection Mach number and pressure.

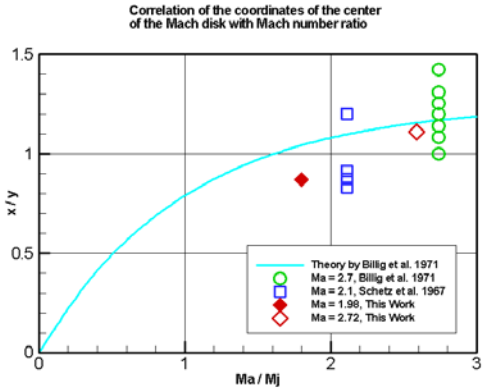

Fig. 13: The coordinates of the center of the Mach disk as a function of the Mach number ratio. x and y are the coordinates of the Mach disk location. M_a, M_j are the Mach numbers of the free stream and the injectant, respectively.

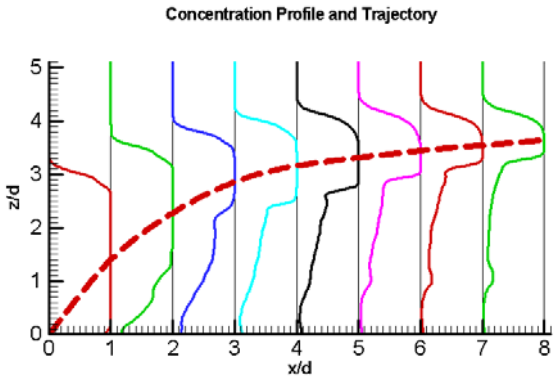

Fig. 14: Jet trajectory and injectant concentration profiles at location x = 1d, 2d, …, and 8d. The free stream Mach number is 1.98 [1].

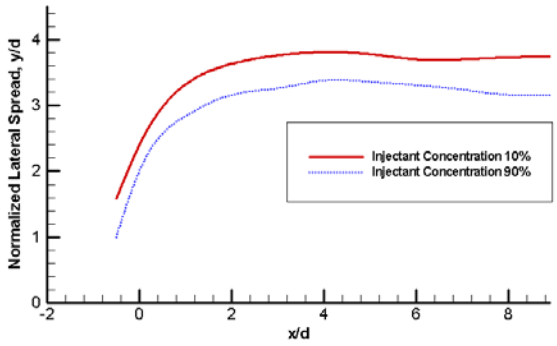

Fig. 15: Injectant lateral spread for the case of M_a = 1.98 [1].

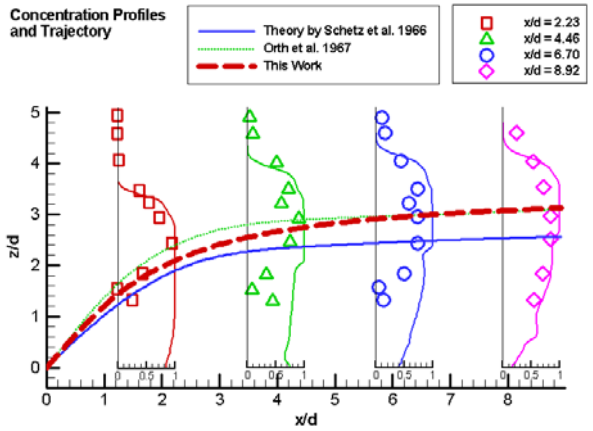

Fig. 16: Jet trajectory and injectant concentration profiles. In the four embedded small figures, the symbols present experimental data by Orth et al. 1967, the lines stand for the result of present work. For the jet trajectory, the present CFD results compared well with the theoretical trajectory by Schetz et al. [4], and the experimental data by Orth et al. [3]. Note that the flow condition follows that in [3] and the free stream Mach number is 2.72